

# Resting-State Functional Connectivity Does Not Predict Individual Differences in Perceived Psychological Stress Among Midlife Adults: Evidence From a Preregistered Cross-Validation Study

Chrystal Spencer, MS, Javier Rasero, PhD, Rebecca G. Reed, PhD,  
Timothy D. Verstynen, PhD, and Peter J. Gianaros, PhD

**Objective:** It is theorized that appraisals of perceived psychological stress are represented in the brain. However, a neural signature that reliably predicts perceived stress has yet to be fully characterized. Accordingly, the present preregistered study tested whether whole-brain resting-state functional connectivity patterns predict individual differences in perceived stress.

**Methods:** Participants ( $N = 417$ ; 53% female; 24.2% non-White; aged 30–54 years) completed the 10-item Perceived Stress Scale and underwent a 5-minute resting-state functional magnetic resonance imaging scan. Functional connectivity (FC) was computed between areas distributed across the brain. In total, 19,900 functional connections (edges) were retained for analyses. Cross-validated and multivariate machine learning methods were implemented. Using this approach, two penalized regression models with cross-validation—elastic net and ridge—were conducted to predict perceived stress from the edges.

**Results:** Across the elastic net and ridge regression models, whole-brain resting-state FC patterns failed to predict individual differences in perceived stress. However, in exploratory analyses, they successfully generalized in cross-validation to predict age for both models (elastic net:  $r = 0.193$ ,  $p < .0001$ , 95% CI = 0.099–0.284, RMSE = 6.661, MAE = 5.715,  $R^2 = 0.037$ ; ridge:  $r = 0.197$ ,  $p < .0001$ , 95% CI = 0.103–0.287), RMSE = 6.613, MAE = 5.8140,  $R^2 = 0.039$ ).

**Conclusion:** These results suggest that resting-state FC patterns may not reliably predict individual differences in self-reported perceived stress among midlife adults.

**Key words:** perceived stress, resting-state functional connectivity, penalized regression, cross-validation

**Abbreviations:** ACC = anterior cingulate cortex, AHAB = Adult Health and Behavior study, AI = anterior insula, BF = Bayes factor, FC = functional connectivity, fMRI = functional magnetic resonance imaging, FWD = framewise displacement, LASSO = least absolute shrinkage and selection operator, MAE = mean absolute error,

PIP = Pittsburgh Imaging Project, PSS = Perceived Stress Scale, RMSE = root mean square error, ROI = region of interest, vmPFC = ventromedial prefrontal cortex

(*Biopsychosoc Sci Med* 2025;87:138–145)

## INTRODUCTION

According to the stage model of stress and disease (1), events and contexts that are appraised as stressful, that is, threatening and taxing to one's ability to cope (2), lead to affective, behavioral, and physiological responses that may culminate in increased risk for physical disease (3). Taken together, these responses are thought to comprise major dimensions of states of psychological stress. Psychological stress itself is typically assessed by self-report inventories (e.g., Perceived Stress Scale; PSS) (4). Not all individuals, however, appraise the same events or contexts similarly, and hence, there is wide variation across individuals on these measures of perceived psychological stress (hereafter “perceived stress”). Importantly, these individual differences in perceived stress are associated with commensurate variation in biological and behavioral risk factors for disease (e.g., inflammation, health-damaging coping behaviors, etc.), as well as clinical conditions and outcomes (e.g., cardiovascular, cerebrovascular, and metabolic diseases) (5–13). A long-standing yet untested assumption of models of psychological stress and physical health is that the brain generates stress appraisals and bodily states, which are linked to downstream influences on health (1). However, a neural signature that reliably predicts perceived stress has yet to be fully characterized. As such, the goal of the present study was to identify brain systems and functional neural metrics that may relate reliably to individual differences in perceived stress.

It is likely that perceived stress is represented in the brain by activity between multiple prefrontal and medial temporal regions that are involved in the affective, behavioral, and physiological dimensions of the stress response (14, 15), including the ventromedial prefrontal cortex (vmPFC), anterior insula (AI), anterior cingulate cortex (ACC), amygdala, and hippocampus. Several of these regions are components of anatomically and functionally interconnected brain systems that are implicated in neuroendocrine, visceromotor, and behavioral phenomena (15–22), including processes relevant to perceived stress. Most of the existing evidence from the human neuroimaging literature suggests that acute stress engages these regions. Specifically, activity in the vmPFC, AI, and ACC has been associated with measures of stressor-evoked cardiovascular reactivity,

From the Department of Psychology (Spencer, Reed, Gianaros), University of Pittsburgh, Pittsburgh, Pennsylvania; School of Data Science (Rasero), University of Virginia, Charlottesville, Virginia; Department of Psychology & Neuroscience Institute (Verstynen), Carnegie Mellon University, Pittsburgh, Pennsylvania.

Address correspondence to Chrystal Spencer, MS, Department of Psychology, University of Pittsburgh, Old Engineering Hall, 3943 O'Hara St, Pittsburgh, PA 15213. E-mail: chrystal.spencer@pitt.edu

ORCID IDs: <https://orcid.org/0000-0001-7105-7141> (C.S.); <https://orcid.org/0000-0003-1661-2856> (J.R.); <https://orcid.org/0000-0003-0794-594X> (R.G.R.); <https://orcid.org/0000-0003-4720-0336> (T.D.V.); <https://orcid.org/0000-0003-2313-5277> (P.J.G.)

Article Editor: Nina Kupper

Received for publication April 25, 2024; revision received October 27, 2024.

Supplemental digital content is available for this article.

Copyright © 2025 Society for Biopsychosocial Science and Medicine

ISSN: 2998-8748

DOI: 10.1097/PSY.0000000000001358

including heart rate, blood pressure, and cardiac output (23–30). Individual differences in these metrics have been associated with volumetric alterations in the amygdala and hippocampus (31,32). Acute stress also appears to modulate the functional connectivity (FC) patterns of these brain systems (27,33–37). Further, there is mounting evidence showing that chronic stress similarly relates to modulations in the structure (38,39) and resting-state FC patterns (40–47) of these brain regions, suggesting that they may also be involved in the processing of stressors in a more chronic, ambient context. In a similar vein, these brain systems have been implicated in stress-related psychopathology, such as posttraumatic stress disorder and mood disorders (48–62).

Although they contribute greatly to our understanding of the neural bases of stress, these and other brain-wide association studies have analytical and inferential limitations (14) that preclude inferences about reliable functional neural correlates of individual differences in perceived stress. A major drawback is that in using the standard mass-univariate analytic approach, many of them inaccurately assume that the neural effects of stress are localized to one or a few brain regions and thus treat them as independent observations in statistical models. Testing such inferences requires multiple comparisons correction, which can be problematic if sample sizes are inadequate and assumptions about independence are incorrect (63). It is more plausible that psychological phenomena, including psychological stress, are encoded in multiple distributed brain systems, rather than one or a few select brain regions (64–69). Accordingly, the primary prediction tested here is that FC patterns across the brain will predict individual differences in perceived stress. Examining this question requires a more robust analytic approach, namely, multivariate predictive modeling (70,71), which would be more suitable for characterizing a neural signature comprised of functional connections across the brain that reliably predict perceived stress. Only one study to date has directly addressed the question tested in the present study using such an approach. Liu and colleagues showed that among college-aged adults, individual differences in perceived stress during the COVID-19 pandemic were predicted by resting-state FC patterns between brain systems related to stress processing (72).

The present preregistered study has similarly aimed to determine whether individual differences in perceived stress are reliably predicted by whole-brain resting-state FC patterns in a sample of over 400 midlife adults. To achieve this, we used a multivariate machine learning approach, which combined predictor dimensionality reduction, penalized regression, and cross-validation. In the predictive model, all functional connections, or *edges*, in the whole-brain resting-state patterns were used to predict individual differences in perceived stress. Using nested cross-validation and accounting for correlated variation across functional brain connections, the model was iteratively trained and tested using subsets of study participants. Critically, testing was always done on an out-of-sample subset not used for training, which allowed us to evaluate the model's predictive ability and to determine whether it is generalizable, that is, whether it could be used to predict outcomes on novel datasets (73). This approach is in line with current best practices in multivariate brain-wide association studies (74) and can help to address power issues, namely, in-sample effect size

inflation and lack of replicability, in samples of moderate sizes ( $n = 75$ –500 subjects) (75).

## METHODS

### Participants

Participants were recruited as part of two projects: the Pittsburgh Imaging Project (PIP;  $n = 331$ , age 30–51 years) and Phase II of the Adult Health and Behavior project (AHAB;  $n = 107$ , age 30–54 years). Eligibility was based on the following exclusion criteria: history of chronic medical illness (e.g., diabetes, cancer, emphysema, rheumatological conditions, etc.), cardiovascular or cerebrovascular disease, or psychiatric or neurological disorder; use of medications with known cardiovascular or autonomic effects; use of psychotropic medications; presence of standard MRI contraindications (i.e., claustrophobia, presence of metal in or on the body/history of metal exposure); pregnancy; consumption of  $\geq 5$  servings of alcohol 3 or more times/week; treatment for hypertension, or having a resting blood pressure greater than 140/60 mm Hg; left-handedness; and color-blindness. Given that the functional magnetic resonance imaging (fMRI) data acquisition protocol was identical for both studies, PIP and AHAB participants were combined to maximize statistical power. To retain as much of the full sample as possible, missing values on variables of interest ( $< 1\%$  missingness across variables) were median imputed. Twenty-one participants with mean framewise displacement (FWD; a measure of head motion over time during fMRI data acquisition) of  $\geq 0.5$  mm were excluded from the analyses. The final analytic sample was 417 participants. As noted above, coupled with a robust cross-validation method, this moderately sized sample is sufficient for obtaining unbiased effect sizes (75).

### Procedure

All participants provided written informed consent, and experiments were conducted in accordance with protocols approved by the University of Pittsburgh Institutional Review Board. Before access to the data was granted, the study hypotheses and analytic plan were preregistered through the Open Science Framework in adherence to their disclosure requirements. Data collection for variables of interest in the current study was completed between 2008 and 2011. Participants completed a series of visits that included anthropometric and psychophysiological measurements; questionnaires related to their medical and demographic history, psychosocial characteristics (e.g., PSS), and intellectual ability; and an MRI scan. Due to variability in participant scheduling, the PSS and MRI scan were completed on separate visits for the AHAB cohort, whereas most participants in the PIP cohort completed these assessments during the same visit. On average, the time between measures across the two cohorts was 4 days ( $SD = 11.72$ ; range, 0–80 days).

### Perceived Stress

Perceived stress was assessed using the 10-item Perceived Stress Scale (PSS-10). This scale offers a global measure of the extent to which a person appraises their life events over the last month as stressful. An example item is, "In the last month, how

often have you been upset because of something that happened unexpectedly?" For each item, participants rate the frequency with which they have experienced the feeling or thought described on a scale from 0 (Never) to 4 (Very Often). It has both high internal reliability ( $\alpha = .85$  in PIP,  $\alpha = .89$  in AHAB) and high test-retest reliability (intraclass correlation  $> 0.70$ ) (76). The PSS has been shown to be a better predictor of health outcomes (e.g., life event scores, depressive and physical symptomatology, anxiety, health behaviors) than more specific life event scales (4). The highest score on the PSS-10 is 40, and higher scores indicate higher levels of perceived stress.

## fMRI Acquisition and Preprocessing

fMRI data for both PIP and AHAB were acquired by the same scanner, specifically a 3T Trio TIM whole-body MRI system (Siemens, Erlangen, Germany), equipped with a 12-channel phased-array head coil. Participants laid in the scanner for 5 minutes with their eyes open (a commonly used scanning duration that has been shown to yield stable functional connectivity metrics (77,78)), whereas blood-oxygen level-dependent (BOLD) images with a gradient-echo EPI sequence were acquired using the following parameters: TR = 2000 milliseconds, TE = 28 milliseconds, flip angle = 90 degrees, field of view =  $205 \times 205 \text{ mm}^2$ , matrix size =  $64 \times 64 \text{ mm}^2$ , 39 slices, and 3-mm isotropic voxels. Slices were obtained using an interleaved sequence in the inferior-to-superior direction, yielding 150 total BOLD images. The first three images were discarded to allow for magnetic equilibration. T1-weighted 3D magnetization-prepared rapid gradient echo neuroanatomical images were acquired over a duration of 7 minutes 17 seconds with the following parameters: FOV =  $256 \times 208 \text{ mm}^2$ , matrix size =  $256 \times 208 \text{ mm}^2$ , and TR = 2100 milliseconds.

The following preprocessing procedures, adapted from a separate analysis project previously carried out in PIP (79), were similarly applied to both PIP and AHAB cohorts. Resting-state BOLD data were preprocessed using the CONN toolbox (80) following a standard fMRI preprocessing pipeline, with steps including realignment using a six-parameter rigid-body transformation, co-registration to the T1-weighted structural image, and normalization to MNI space. Additionally, to further reduce noise in the data, the following additional preprocessing steps were implemented: temporal bandpass filtering ( $0.009 \text{ Hz} < f < 0.08 \text{ Hz}$ ), spatial smoothing of functional images using a 6-mm full-width-at-half-maximum Gaussian kernel, and regression of motion and physiological noise in a model including regressors derived from the six parameters from the realignment step and regressors for CSF, white matter, and global brain signal (81).

## Functional Connectivity Computation

The denoised data were then segmented. In the original preregistration, we proposed to use a whole-brain fMRI parcellation comprising 268 regions to compute FC (82). However, in preliminary analyses, several FC values could not be computed due to poor coverage in the cerebellum within our data. As such, we revised the preregistration, and segmentation of the denoised data was instead based on a 200-region whole-brain fMRI parcellation (83). Resting-state derived atlases are preferred over the standard anatomical atlases (e.g., AAL).

First, the anatomical/cytoarchitectural homogeneity of regions as defined by standard atlases does not necessarily extend to patterns of connectivity. Different subregions of a given structure may be networked with distinctly different regions, and thus may be implicated in different cognitive functions (83). Thus, atlases like the AAL may not be suitable for resting-state FC analyses.

Functional connectivity was computed in the CONN toolbox using the ROI-to-ROI approach. For each pair of parcels, bivariate Pearson correlation coefficients were computed for the BOLD timeseries. These coefficients were then transformed using Fisher Z transformation. The upper triangle of the resulting connectivity matrix, which was retained for analyses, consisted of 19,900 correlations (edges) per participant.

## Machine Learning Analyses

All statistical analyses were performed using R Statistical Software v3.1.0 (84), utilizing the caret (v6.0.94) (85), glmnet (v4.1.8) (86), and BayesFactor (v0.9.12.4.7) (87) packages. We used a multivariate penalized regression approach to test whether perceived stress was predicted by whole-brain resting-state FC patterns. In this analysis, all 19,900 edges were the multivariate predictor variables, and the PSS score was the outcome variable. First, to reduce the dimensionality of the input data and address concerns of multicollinearity, principal components analysis was applied to the normalized and scaled edges. This operation transformed the input features (i.e., the edges) to the principal component space whose dimensionality was  $n - 1$ , with  $n$  being the number of participants within a given training set split. Next, perceived stress was regressed onto the principal components using penalized regression models. Our primary model was the elastic net model because it combines the penalty terms of the Least Absolute Shrinkage and Selection Operator (LASSO) (L1) and ridge (L2) regression models. Briefly, when applied, these penalties shrink high variance beta coefficients to or toward zero, respectively. These effects are modulated by two hyperparameters: a shrinkage parameter  $\lambda$ , which determines how much penalization is applied (ranges from 0 to  $\infty$ ), and a mixing parameter  $\alpha$ , which determines the ratio of L1 and L2 penalties ( $\alpha = 0$  for ridge [L2],  $\alpha = 1$  for LASSO [L1],  $0 < \alpha < 1$  for elastic net). We also ran ridge regression as our secondary model, given its treatment of multicollinearity, as it reconciles correlated predictors by shrinking them near each other rather than removing one of them from the model (88). LASSO regression, on the other hand, proved to be too stringent in this analysis context, removing too many features and thus preventing the model from converging (results not reported here) (89).

Nested  $k$ -fold cross-validation was implemented, where the model's predictive ability was assessed within the outer loop and the model hyperparameters were optimized within the inner loop (90). In the outer loop, 10-fold cross-validation was implemented, such that the dataset was partitioned into 10 nonoverlapping subsets of equal size. At each fold, all but one of these subsets were used for model training (training set), and the held-out subset was used for model testing (i.e., testing set). Then, the training set was passed to the inner loop for hyperparameter tuning, where a range of  $\lambda$  and  $\alpha$  values

were tested via grid search to find the optimal parameters—namely, those values that minimize the prediction error. Within this inner loop, five-fold cross-validation was implemented with the same data partitioning process described above. For the elastic net model, a range of 100  $\lambda$  values from 0 to 100 and  $\alpha$  values 0, .5, and 1 were tested. For the ridge model, a range of 100  $\lambda$  values from 0 to 25 were tested and  $\alpha$  was fixed at 0. The hyperparameter tuning process was repeated three times to test the reliability of the resulting model performance metrics. These optimized hyperparameters were then used to train the model and generate predictions in the held-out testing set from the outer loop.

The final predictive performance of each model concatenated across the outer folds was summarized by multiple metrics, per recommendations on best practices for reporting predictive modeling results (74). The differences between predicted and observed PSS scores were summarized by the root mean squared error (RMSE) and mean absolute error (MAE) values. The proportion of variance in the predicted values explained by the observed values was summarized by the coefficient of determination ( $R^2$ ), which was computed using the sums of squares formula. The association between predicted and observed PSS scores was summarized by the Pearson correlation coefficient, along with the corresponding  $p$  value and 95% CI. To facilitate interpretations of results that did not reach statistical significance by conventional standards, Bayes factors (BF) were computed.  $BF_{10}$  and  $BF_{01}$  values quantify the evidence in favor of the alternative and null hypotheses, respectively. Code for analysis and results for all models are available upon request.

In addition to those that were preregistered, we also conducted several exploratory analyses using the same approach described above. We stratified the sample by sex and cohort to test for differential predictive relationships based on these variables. We also tested the predictive models within two subsets of participants: a) those who completed the PSS and MRI within a month of each other (i.e., a time difference of 31 days or less;  $N = 403$ ), given that the PSS is anchored over the past month and the wide variability in time between measures in this sample; and b) those with “high” levels of perceived stress, defined as having a PSS score comparable to that observed in Liu et al. (72) (i.e., a PSS score of 21.5 or higher;  $N = 50$ ). Finally, as a pipeline check, we tested whether age was predicted by whole-brain resting-state FC patterns, as this has been found previously (91–93), by replacing age as the outcome variable in the predictive models.

## RESULTS

### Sample Characteristics and Associations Among Model Variables

Table 1 outlines characteristics of the analytic sample ( $n = 417$ ). Participants were a mean age of 41 years, 53% female, and 24.2% non-White. This sample had relatively low perceived stress (mean = 13.8; SD = 6.0) but showed adequate variability (observed range: 0–32). Participants with FWD outlier values reported, on average, higher perceived stress than those included in the analyses (17.8 versus 13.8,  $t(436) = 2.86, p = .009$ ), but they did not differ on age. Partici-

**TABLE 1.** Analytic Sample Characteristics— $N = 417$  (95%)

Characteristics	AHAB ( $N = 106$ )	PIP ( $N = 311$ )	Overall ( $N = 417$ )
Female (%)	62.3	49.8	53
Race (%)			
White	83	73.3	75.8
Black	12.3	20.6	18.5
Asian	4.7	4.2	4.3
Native American	0	1	.7
Bi/Multiracial	0	1	.7
Other	0	0	0
Age (y)	41.9 (7.99)	40.8 (6.23)	41 (6.73)
PSS score (out of 40)	13.7 (6.08)	13.8 (5.99)	13.8 (6.00)
Framewise displacement (mm)	0.16 (0.08)	0.17 (0.09)	0.17 (0.08)

AHAB = Adult Health and Behavior study; PIP = Pittsburgh Imaging Project; PSS = Perceived Stress Scale.

Values reflect mean (standard deviation), unless otherwise noted.

pants in PIP and AHAB did not differ on age, perceived stress, or FWD. Age was correlated with FWD ( $r = 0.12, p = .019$ ), but not perceived stress. Female participants were slightly older than male participants (mean age = 42.00 versus 40.01 years),  $t(411) = -2.997, p = .003$ , but there were no sex differences in PSS score or FWD.

### Predictive Modeling Results

Using a cross-validated penalized regression approach, we found that the models predicting perceived stress performed poorly. As depicted in Figure 1, nested cross-validation showed that perceived stress predicted by whole-brain resting-state FC patterns was not significantly correlated with observed PSS scores: elastic net:  $r = -.035, p = .479, 95\% \text{ CI} = -0.131$  to  $0.061, \text{RMSE} = 6.441, \text{MAE} = 5.095, R^2 = 0.001, BF_{10} = 0.147, BF_{01} = 6.819$ ; ridge:  $r = -0.046, p = .346, 95\% \text{ CI} = -0.142$  to  $0.050, \text{RMSE} = 6.049, \text{MAE} = 4.810, R^2 = 0.002, BF_{10} = 0.178, BF_{01} = 5.637$ . These results do not appear to differ by sex (Figures S1 and S2 in the Supplemental Digital Content, <http://links.lww.com/PSYMED/B55>), cohort (Figures S3 and S4 in the Supplement), time between assessments, or stress level. However, the results of the pipeline check showed that the positive association between age predicted by whole-brain resting-state FC patterns and observed age was significant: elastic net:  $r = 0.193, p < .0001, 95\% \text{ CI} = 0.099$  to  $0.284, \text{RMSE} = 6.661$  years,  $\text{MAE} = 5.715$  years,  $R^2 = 0.037, BF_{10} = 268.360, BF_{01} = 0.004$ ; ridge:  $r = 0.197, p < .0001, 95\% \text{ CI} = 0.103$  to  $0.287, \text{RMSE} = 6.613$  years,  $\text{MAE} = 5.814$  years,  $R^2 = 0.039, BF_{10} = 363.460, BF_{01} = 0.003$  (Figure 2).

## DISCUSSION

In the present study, we were unable to demonstrate that individual differences in perceived stress can be reliably predicted by whole-brain resting-state FC patterns. Cross-validated multivariate penalized regression models performed poorly, and predicted values did not significantly associate with observed values (Figure 1). However, these models did

## Whole-brain resting-state FC patterns do not predict PSS scores

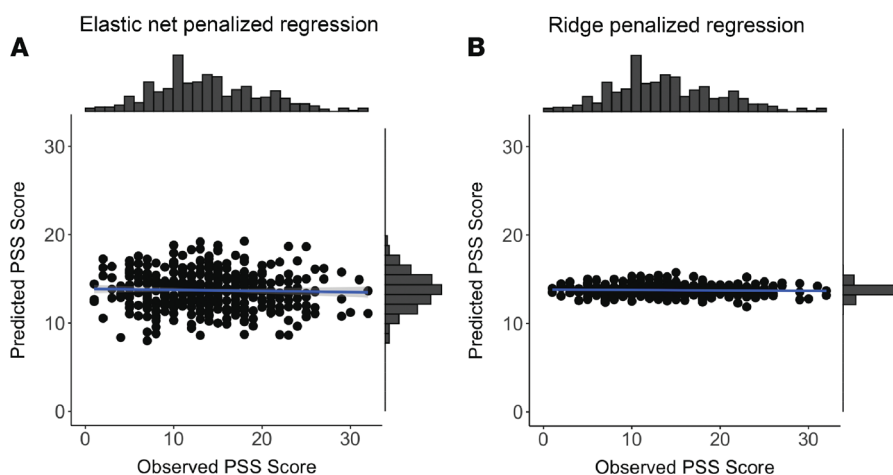


**FIGURE 1.** Relationship between observed and predicted PSS score for two multivariate penalized regression models—(A) elastic net and (B) ridge. Blue solid line and shading represent the lines of best fit and the corresponding 95% confidence interval, respectively. Marginal histograms reflect frequency distributions for observed (on *x* axis) and predicted (on *y* axis) PSS score.

successfully predict age in this sample (Figure 2). Our results suggest that the functional neural correlates of perceived stress may not be reliably characterized by patterns of resting-state FC. Below, we speculate about potential explanations for these findings, including differences in how resting-state FC and perceived stress are operationalized and measured; methodological differences from previous work; robustness of the statistical approach; and low statistical power.

Although existing evidence demonstrates that resting-state FC and perceived stress, as measured in the present study, both exhibit reliable individual differences, it could be that they are conceptually distinct from one another and thus may not be meaningfully related to each other in this context. Perceived stress, for example, is thought to reflect a cumulative “cognitive average” of stress appraisals over the last month. Resting-state FC, on the other hand, is thought to reflect spontaneously

evoked intrinsic brain activity that may be context independent of fluctuating stress appraisals over the past month. Thus, resting-state FC could be capturing underlying at-the-moment processes that may be unrelated to those presumably reflected in the month-aggregated PSS score, and may therefore not be the best measure for modeling individual differences in perceived stress. This may especially be the case given that these measures were obtained, on average, a month apart in the present study (see the Procedures section in Methods). As such, future studies might reconcile these conceptual and operational differences by using an adapted protocol that is in line with the so-called third-wave of human neuroimaging research, which combines the flexibility afforded by resting-state paradigms with the structure of task-based paradigms to improve the interpretability of our results and deepen our understanding of brain-phenotype relationships (94). In this vein, rather than completing an

## Whole-brain resting-state FC patterns predict age

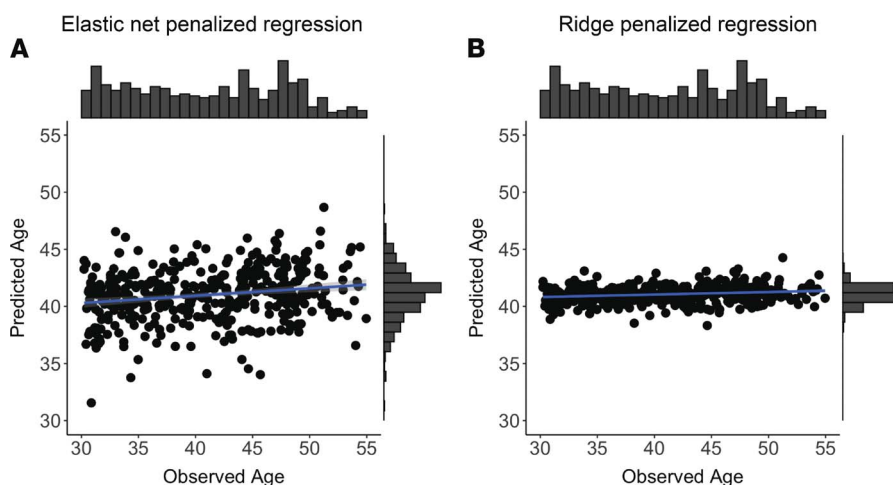


**FIGURE 2.** Relationship between observed and predicted age for two multivariate penalized regression models—(A) elastic net and (B) ridge. The blue solid line and shading represent the lines of best fit and the corresponding 95% confidence interval, respectively. Marginal histograms reflect frequency distributions for observed (on *x* axis) and predicted (on *y* axis) age.

unstructured resting-state scan, participants could instead receive instructions that mirror the items on the PSS (e.g., “During this resting period, think about how unpredictable, uncontrollable, or overloading your life experiences over the last month have been.”). This instruction manipulation may evoke the same cognitions and engage the relevant appraisal processes that are presumably at play during the completion of the PSS. Such an approach involving contemporaneous measurement of appraisal-related cognitions and brain activity would enable a more direct comparison of the two and contribute toward a more precise characterization of the functional neural correlates of perceived stress.

The null findings observed here (which are confirmed by the  $BF_{10}$  values within the range of 1/10–1/3, suggesting moderate evidence in favor of the null hypothesis (95)) could be due to methodological differences between our study and the existing literature. First, Liu and colleagues used a sample of college-aged adults newly experiencing a novel global pandemic (mean age = 19.14 years across the three datasets) (72), whereas our sample consisted of midlife adults studied prior to this historical epoch (mean age = 41 years). Thus, it may be that the association between perceived stress and resting-state FC is an age-dependent effect or one that is dependent on ambient levels of commonly experienced psychological stress (i.e., state-dependent). Moreover, perceived stress appears to decrease with age normatively, with self-reported levels peaking in young adulthood and gradually decreasing into midlife (96,97). This developmental change is reflected in the perceived stress levels observed across the two studies; the college-aged sample in Liu et al. had moderately high levels of perceived stress (mean PSS score = 21.7 across three datasets) (72), whereas our sample of midlife adults had relatively lower levels of perceived stress (mean PSS score = 13.8). Additionally, age-related changes in resting-state FC dynamics are characterized by reduced connectivity within large-scale networks (including the default mode and salience networks) and enhanced connectivity between them (98–100). Differences in the resting-state scan protocols between studies may also account for the discrepancy in results; although Liu et al. had an 8-minute, eyes-closed resting-state scan, our protocol included a 5-minute, eyes-open resting-state scan (72). There is evidence suggesting that both scan length and eye state can influence the connectivity measures obtained. Specifically, the reliability of FC measures is improved with scans of moderate length (~12 minutes) and eyes-open protocols, compared to shorter scans (~5 minutes) (101) and eyes-closed protocols (102,103), respectively. An additional complication with eyes-closed protocols is that they increase the likelihood that participants will fall asleep, which can confound resting-state activity patterns observed. As such, although Liu et al. had a more optimal scan length, our use of an eyes-open scan protocol yielded data that may be more reliable.

Furthermore, differences in statistical approach, coupled with low statistical power, may also explain the failure to replicate the previously published effect. Liu and colleagues used leave-one-out cross-validation, whereas we used nested  $k$ -fold cross-validation (72). In leave-one-out cross-validation, the model is trained on all but one datapoint in the sample, which is retained for subsequent model testing. Though this approach is exhaustive, using almost the entire sample to train the model and thus producing unbiased estimates, the variance between

the resulting model predictions tends to be high, increasing the risk of overfitting (104). Conversely, nested  $k$ -fold cross-validation (described above) attempts to rectify this bias-variance tradeoff by separating the model tuning and model testing processes (90,105). Thus, it may be the more robust approach to using resting-state FC to model individual differences, as demonstrated by the model’s successful prediction of age in our exploratory analyses (Figure 2). Additionally, though the sample size in Liu et al. was double that of the present study ( $n = 817$  versus  $n = 417$ ), it may be the case that both studies are underpowered to detect a replicable effect. By some accounts, multivariate brain-wide association studies require large sample sizes, possibly upward of 1000 participants, to yield replicable results, although some show replicable effects in small to moderate samples (e.g.,  $n = 75$ –500) (63,75,106). Nevertheless, the utilization of cross-validation methods in the present study ensures that the effect sizes observed are unlikely to be biased.

The existing literature on the neural bases of psychological stress is extensive (23–47) but is characterized by inherent analytic and inferential limitations that accompany the mass-univariate analytic approach (14,63). By comparison, there are few studies using predictive modeling to characterize the functional neural correlates of psychological stress (72). None of the present findings suggest that there is a cross-validated predictive signature of perceived stress that accounts for correlated variation in the functionality of distributed brain systems. As such, the results of past studies should be interpreted with caution.

In conclusion, our results suggest that whole-brain resting-state FC patterns do not reliably predict individual differences in perceived stress. It remains unclear whether these results are due to inconsistencies between studies with respect to measurement of model variables, lifespan considerations, methodological approaches, or low statistical power. Future studies using different imaging assessment methods or possibly different markers of chronic psychological stress are warranted to better understand the role of the brain in linking stress and physical health outcomes.

*Source of Funding and Conflicts of Interest:* This work was supported by the National Institutes of Health (NHLBI P01-HL040962 and T32-HL07560). The authors have no conflicts of interest to report.

*Open Science:* The aims, hypotheses, and analysis plan were preregistered through the Open Science Framework.

## REFERENCES

- Cohen S, Gianaros PJ, Manuck SB. A stage model of stress and disease. *Perspect Psychol Sci* 2016;11:456–63.
- Lazarus RS. *Psychological Stress and the Coping process*. New York, NY: McGraw-Hill; 1966.
- Cohen S, Kessler RC, Gordon LU, editors. *Measuring Stress: A Guide for Health and Social Scientists*. New York, NY: Oxford University Press; 1995. xii:236.
- Cohen S, Kamarck T, Mermelstein R. A global measure of perceived stress. *J Health Soc Behav* 1983;24:385.
- Cohen S, Janicki-Deverts D, Miller GE. Psychological stress and disease. *JAMA* 2007;298:1685.
- Dimsdale JE. Psychological stress and cardiovascular disease. *J Am Coll Cardiol* 2008;51:1237–46.
- Everson-Rose SA, Lewis TT. Psychosocial factors and cardiovascular diseases. *Annu Rev Public Health* 2005;26:469–500.
- Kivimäki M, Bartolomucci A, Kawachi I. The multiple roles of life stress in metabolic disorders. *Nat Rev Endocrinol* 2023;19:10–27.

9. Kivimäki M, Steptoe A. Effects of stress on the development and progression of cardiovascular disease. *Nat Rev Cardiol* 2018;15:215–29.
10. Knight EL, Jiang Y, Rodriguez-Stanley J, Almeida DM, Engeland CG, Zilioli S. Perceived stress is linked to heightened biomarkers of inflammation via diurnal cortisol in a national sample of adults. *Brain Behav Immun* 2021;93:206–13.
11. Ng DM, Jeffery RW. Relationships between perceived stress and health behaviors in a sample of working adults. *Health Psychol* 2003;22:638–42.
12. Weiss JM. Psychological factors in stress and disease. *Sci Am* 1972;226:104–13.
13. Yusuf S, Hawken S, Ōunpuu S, Dans T, Avezum A, Lanas F, et al. Effect of potentially modifiable risk factors associated with myocardial infarction in 52 countries (the INTERHEART study): case-control study. *Lancet* 2004;364:937–52.
14. Westlin C, Theriault JE, Katsumi Y, Nieto-Castanon A, Kucyi A, Ruf SF, et al. Improving the study of brain-behavior relationships by revisiting basic assumptions. *Trends Cogn Sci* 2023; 27:246–57.
15. Koban L, Gianaros PJ, Kober H, Wager TD. The self in context: brain systems linking mental and physical health. *Nat Rev Neurosci* 2021;22:309–22.
16. Benarroch EE. The central autonomic network: functional organization, dysfunction, and perspective. *Mayo Clin Proc* 1993;68:988–1001.
17. Gianaros PJ, Wager TD. Brain-body pathways linking psychological stress and physical health. *Curr Dir Psychol Sci* 2015;24:313–21.
18. Ginty AT, Kraynak TE, Fisher JP, Gianaros PJ. Cardiovascular and autonomic reactivity to psychological stress: neurophysiological substrates and links to cardiovascular disease. *Auton Neurosci* 2017;207:2–9.
19. McEwen BS, Gianaros PJ. Central role of the brain in stress and adaptation: links to socioeconomic status, health, and disease: central links between stress and SES. *Ann N Y Acad Sci* 2010;1186:190–222.
20. Saper CB. The central autonomic nervous system: conscious visceral perception and autonomic pattern generation. *Annu Rev Neurosci* 2002;25:433–69.
21. Thayer JF, Hansen AL, Saus-Rose E, Johnsen BH. Heart rate variability, prefrontal neural function, and cognitive performance: the neurovisceral integration perspective on self-regulation, adaptation, and health. *Ann Behav Med* 2009;37:141–53.
22. Vaccarino V, Shah AJ, Mehta PK, Pearce B, Raggi P, Bremner JD, et al. Brain-heart connections in stress and cardiovascular disease: implications for the cardiac patient. *Atherosclerosis* 2021;328:74–82.
23. Beissner F, Meissner K, Bar KJ, Napadow V. The autonomic brain: an activation likelihood estimation meta-analysis for central processing of autonomic function. *J Neurosci* 2013;33: 10503–11.
24. Eisenbarth H, Chang LJ, Wager TD. Multivariate brain prediction of heart rate and skin conductance responses to social threat. *J Neurosci* 2016;36:11987–98.
25. Gianaros PJ, Derbyshire SWG, May JC, Siegle GJ, Gamalo MA, Jennings JR. Anterior cingulate activity correlates with blood pressure during stress. *Psychophysiology* 2005;42:627–35.
26. Gianaros PJ, Jennings JR, Sheu LK, Derbyshire SWG, Matthews KA. Heightened functional neural activation to psychological stress covaries with exaggerated blood pressure reactivity. *Hypertension* 2007;49:134–40.
27. Gianaros PJ, Onyewuanyi IC, Sheu LK, Christie IC, Critchley HD. Brain systems for baroreflex suppression during stress in humans. *Hum Brain Mapp* 2012;33:1700–16.
28. Gianaros PJ, Sheu LK, Uyar F, Koushik J, Jennings JR, Wager TD, et al. A brain phenotype for stressor-evoked blood pressure reactivity. *J Am Heart Assoc* 2017;6:e006053.
29. Ginty AT, Gianaros PJ, Derbyshire SWG, Phillips AC, Carroll D. Blunted cardiac stress reactivity relates to neural hypoactivation. *Psychophysiology* 2013;50:219–29.
30. Wager TD, Waugh CE, Lindquist M, Noll DC, Fredrickson BL, Taylor SF. Brain mediators of cardiovascular responses to social threat. *Neuroimage* 2009;47:821–35.
31. Gianaros PJ, Sheu LK, Matthews KA, Jennings JR, Manuck SB, Hariri AR. Individual differences in stressor-evoked blood pressure reactivity vary with activation, volume, and functional connectivity of the amygdala. *J Neurosci* 2008;28:990–9.
32. Trotman GP, Gianaros PJ, Veldhuijzen van Zanten JCS, Williams SE, Ginty AT. Increased stressor-evoked cardiovascular reactivity is associated with reduced amygdala and hippocampus volume. *Psychophysiology* 2019;56:e13277.
33. Ginty AT, Kraynak TE, Kuan DC, Gianaros PJ. Ventromedial prefrontal cortex connectivity during and after psychological stress in women. *Psychophysiology* [Internet] 2019;56: e13445. doi:10.1111/psyp.13445.
34. Vaisvaser S, Lin T, Admon R, Podlipsky I, Greenman Y, Stern N, et al. Neural traces of stress: cortisol related sustained enhancement of amygdala-hippocampal functional connectivity. *Front Hum Neurosci* [Internet] 2013;7:313. Available at: <http://journal.frontiersin.org/article/10.3389/fnhum.2013.00313/abstract>.
35. van Marle HJF, Hermans EJ, Qin S, Fernández G. Enhanced resting-state connectivity of amygdala in the immediate aftermath of acute psychological stress. *Neuroimage* 2010;53: 348–54.
36. Veer IM, Oei NYL, Spinhoven P, van Buchem MA, Elzinga BM, Rombouts SARB. Beyond acute social stress: increased functional connectivity between amygdala and cortical midline structures. *Neuroimage* 2011;57:1534–41.
37. Quaedflieg CWEM, van de Ven V, Meyer T, Siep N, Merckelbach H, Smeets T. Temporal dynamics of stress-induced alterations of intrinsic amygdala connectivity and neuroendocrine levels. *PLoS One* 2015;10:e0124141.
38. Caetano I, Amorim L, Soares JM, Ferreira S, Coelho A, Reis J, et al. Amygdala size varies with stress perception. *Neurobiol Stress* 2021;14:100334.
39. Hölzel BK, Carmody J, Evans KC, Hoge EA, Dusek JA, Morgan L, et al. Stress reduction correlates with structural changes in the amygdala. *Soc Cogn Affect Neurosci* 2010;5:11–7.
40. Archer JA, Lee A, Qiu A, Annabel Chen SH. Functional connectivity of resting-state, working memory and inhibition networks in perceived stress. *Neurobiol Stress* 2018;8: 186–201.
41. Caetano I, Ferreira S, Coelho A, Amorim L, Castanho TC, Portugal-Nunes C, et al. Perceived stress modulates the activity between the amygdala and the cortex. *Mol Psychiatry* 2022;27:4939–47.
42. Goldfarb EV, Rosenberg MD, Seo D, Constable RT, Sinha R. Hippocampal seed connectome-based modeling predicts the feeling of stress. *Nat Commun* 2020;11:2650.
43. Hanson JL, Albert WD, Skinner AT, Shen SH, Dodge KA, Lansford JE. Resting state coupling between the amygdala and ventromedial prefrontal cortex is related to household income in childhood and indexes future psychological vulnerability to stress. *Dev Psychopathol* 2019;31:1053–66.
44. Taren AA, Gianaros PJ, Greco CM, Lindsay EK, Fairgrieve A, Brown KW, et al. Mindfulness meditation training alters stress-related amygdala resting state functional connectivity: a randomized controlled trial. *Soc Cogn Affect Neurosci* 2015;10:1758–68.
45. Tawakol A, Ishai A, Takx RA, Figueroa AL, Ali A, Kaiser Y, et al. Relation between resting amygdala activity and cardiovascular events: a longitudinal and cohort study. *Lancet* 2017; 389:834–45.
46. Shao R, Lau WKW, Leung MK, Lee TMC. Subgenual anterior cingulate-insula resting-state connectivity as a neural correlate to trait and state stress resilience. *Brain Cogn* 2018;124:73–81.
47. Huang BK, Zhou JH, Deng Y, Li CH, Ning BL, Ye ZY, et al. Perceived stress and brain connectivity in subthreshold depression: insights from eyes-closed and eyes-open states. *Brain Res* 2024;1838:148947.
48. Hopper JW, Frewen PA, van der Kolk BA, Lanius RA. Neural correlates of reexperiencing, avoidance, and dissociation in PTSD: symptom dimensions and emotion dysregulation in responses to script-driven trauma imagery. *J Trauma Stress* 2007;20:713–25.
49. Jeong H, Chung YA, Ma J, Kim J, Hong G, Oh JK, et al. Diverging roles of the anterior insula in trauma-exposed individuals vulnerable or resilient to posttraumatic stress disorder. *Sci Rep* 2019;9:15539.
50. Nicholson AA, Sapru I, Densmore M, Frewen PA, Neufeld RWJ, Théberge J, et al. Unique insula subregion resting-state functional connectivity with amygdala complexes in posttraumatic stress disorder and its dissociative subtype. *Psychiatry Res Neuroimaging* 2016;250:61–72.
51. Pitman RK, Rasmusson AM, Koenen KC, Shin LM, Orr SP, Gilbertson MW, et al. Biological studies of post-traumatic stress disorder. *Nat Rev Neurosci* 2012;13:769–87.
52. Zhang Y, Xie B, Chen H, Li M, Guo X, Chen H. Disrupted resting-state insular subregions functional connectivity in post-traumatic stress disorder. *Medicine (Baltimore)* 2016;95:e4083.
53. Chen HJ, Zhang L, Ke J, Qi R, Xu Q, Zhong Y, et al. Altered resting-state dorsal anterior cingulate cortex functional connectivity in patients with post-traumatic stress disorder. *Aust N Z J Psychiatry* 2019;53:68–79.
54. Conolly CG, Wu J, Ho TC, Hoeft F, Wolkowitz O, Eisendrath S, et al. Resting-state functional connectivity of subgenual anterior cingulate cortex in depressed adolescents. *Biol Psychiatry* 2013;74:898–907.
55. Drevets WC, Savitz J, Trimble M. The Subgenual anterior cingulate cortex in mood disorders. *CNS Spectr* 2008;13:663–81.
56. Holsen LM, Spaeth SB, Lee J-H, Ogden LA, Klibanski A, Whitfield-Gabrieli S, et al. Stress response circuitry hypoactivation related to hormonal dysfunction in women with major depression. *J Affect Disord* 2011;131:379–87.
57. Kennis M, Rademaker AR, van Rooij SJ, Kahn RS, Geuze E. Resting state functional connectivity of the anterior cingulate cortex in veterans with and without post-traumatic stress disorder. *Hum Brain Mapp* 2015;36:99–109.
58. Shin LM, Whalen PJ, Pitman RK, Bush G, Macklin ML, Lasko NB, et al. An fMRI study of anterior cingulate function in posttraumatic stress disorder. *Biol Psychiatry* 2001;50:932–42.
59. Shin LM, Bush G, Whalen PJ, Handwerker K, Cannistraro PA, Wright CI, et al. Dorsal anterior cingulate function in posttraumatic stress disorder. *J Trauma Stress* 2007;20:701–12.
60. van Wingen GA, Geuze E, Vermetten E, Fernández G. Perceived threat predicts the neural sequelae of combat stress. *Mol Psychiatry* 2011;16:664–71.
61. Rabinak CA, Angstadt M, Welsh RC, Kennedy AE, Lyubkin M, Martis B, et al. Altered amygdala resting-state functional connectivity in post-traumatic stress disorder. *Front Psychiatry* 2011;2:62.
62. Sripada RK, King AP, Garfinkel SN, Wang X, Sripada CS, Welsh RC, et al. Altered resting-state amygdala functional connectivity in men with posttraumatic stress disorder. *J Psychiatry Neurosci* 2012;37:241–9.
63. Marek S, Tervo-Clemmens B, Calabro FJ, Montez DF, Kay BP, Hatoum AS, et al. Reproducible brain-wide association studies require thousands of individuals. *Nature* 2022;603:654–60.
64. Knutson B, Taylor J, Kaufman M, Peterson R, Glover G. Distributed neural representation of expected value. *J Neurosci* 2005;25:4806–12.
65. Shin EJ, Jiang Y, Kim S, Kim H, Cai X, Lee H, et al. Robust and distributed neural representation of action values. *Elife* 2021;10:e53045.
66. Baucom LB, Wedell DH, Wang J, Blitzer DN, Shinkareva SV. Decoding the neural representation of affective states. *Neuroimage* 2012;59:718–27.
67. Bush KA, Inman CS, Hamann S, Kilts CD, James GA. Distributed neural processing predictors of multi-dimensional properties of affect. *Front Hum Neurosci* 2017;11:459.
68. Chang LJ, Gianaros PJ, Manuck SB, Krishnan A, Wager TD. A sensitive and specific neural signature for picture-induced negative affect. *PLoS Biol* 2015;13:e1002180.

69. Zhang Z, Fanning J, Ehrlich DB, Chen W, Lee D, Levy I. Distributed neural representation of saliency controlled value and category during anticipation of rewards and punishments. *Nat Commun* 2017;8:1907.
70. Cosme D, Zeithamova D, Stice E, Berkman ET. Multivariate neural signatures for health neuroscience: assessing spontaneous regulation during food choice. *Soc Cogn Affect Neurosci* 2020;15:1120–34.
71. Woo CW, Chang LJ, Lindquist MA, Wager TD. Building better biomarkers: brain models in translational neuroimaging. *Nat Neurosci* 2017;20:365–77.
72. Liu P, Yang W, Zhuang K, Wei D, Yu R, Huang X, et al. The functional connectome predicts feeling of stress on regular days and during the COVID-19 pandemic. *Neurobiol Stress* 2021;14:100285.
73. Rosenbusch H, Soldner F, Evans AM, Zeelenberg M. Supervised machine learning methods in psychology: a practical introduction with annotated R code. *Soc Pers Psychol Compass* 2021;15:e12579.
74. Poldrack RA, Huckins G, Varoquaux G. Establishment of best practices for evidence for prediction: a review. *JAMA Psychiatry* 2020;77:534–40.
75. Spisak T, Bingel U, Wager TD. Multivariate BWAS can be replicable with moderate sample sizes. *Nature* 2023;615:E4–7.
76. Lee EH. Review of the psychometric evidence of the perceived stress scale. *Asian Nurs Res* 2012;6:121–7.
77. Van Dijk KRA, Sabuncu MR, Buckner RL. The influence of head motion on intrinsic functional connectivity MRI. *Neuroimage* 2012;59:431–8.
78. Fox MD, Snyder AZ, Vincent JL, Corbetta M, Van Essen DC, Raichle ME. The human brain is intrinsically organized into dynamic, anticorrelated functional networks. *Proc Natl Acad Sci U S A* 2005;102:9673–8.
79. Kraynak TE, Marsland AL, Hanson JL, Gianaros PJ. Retrospectively reported childhood physical abuse, systemic inflammation, and resting corticolimbic connectivity in midlife adults. *Brain Behav Immun* 2019;82:203–13.
80. Whitfield-Gabrieli S, Nieto-Castanon A. Conn: a functional connectivity toolbox for correlated and anticorrelated brain networks. *Brain Connect* 2012;2:125–41.
81. Power JD, Cohen AL, Nelson SM, Wig GS, Barnes KA, Church JA, et al. Functional network organization of the human brain. *Neuron* 2011;72:665–78.
82. Shen X, Tokoglu F, Papademetris X, Constable RT. Groupwise whole-brain parcellation from resting-state fMRI data for network node identification. *Neuroimage* 2013;82:403–15.
83. Craddock RC, James GA, Holtzheimer PE 3rd, Hu XP, Mayberg HS. A whole brain fMRI atlas generated via spatially constrained spectral clustering. *Hum Brain Mapp* 2012;33:1914–28.
84. R Core Team. R: A Language and Environment for Statistical Computing [Internet]. Vienna, Austria: R Foundation for Statistical Computing; 2023. Available at: <https://www.R-project.org/>.
85. Kuhn M. Building predictive models in R using the caret package. *J Stat Softw* 2008;28:1–26.
86. Friedman J, Hastie T, Tibshirani R. Regularization paths for generalized linear models via coordinate descent. *J Stat Softw* 2010;33:1–22.
87. Morey RD, Rouder JN. BayesFactor: Computation of Bayes Factors for Common Designs [Internet]. 2024. Available at: <https://CRAN.R-project.org/package=BayesFactor>. Accessed March 21, 2024.
88. Khalaf G, Shukur G. Choosing ridge parameter for regression problems. *Commun Stat Theory Methods* 2005;34:1177–82.
89. Zou H, Hastie T. Regularization and variable selection via the elastic net. *J R Stat Soc Ser B Stat Methodol* 2005;67:301–20.
90. Korjus K, Hebart MN, Vicente R. An efficient data partitioning to improve classification performance while keeping parameters interpretable. *PLoS One* 2016;11:e0161788.
91. Kandaleft D, Murayama K, Roesch E, Sakaki M. Resting-state functional connectivity does not predict individual differences in the effects of emotion on memory. *Sci Rep* 2022;12:14481.
92. Tsvetanov KA, Henson RNA, Tyler LK, Razi A, Geerligs L, Ham TE, et al. Extrinsic and intrinsic brain network connectivity maintains cognition across the lifespan despite accelerated decay of regional brain activation. *J Neurosci* 2016;36:3115–26.
93. Vergun S, Deshpande AS, Meier TB, Song J, Tudorascu DL, Nair VA, et al. Characterizing functional connectivity differences in aging adults using machine learning on resting state fMRI data. *Front Comput Neurosci* 2013;7:38.
94. Finn ES. Is it time to put rest to rest? *Trends Cogn Sci* 2021;25:1021–32.
95. Stefan AM, Gronau QF, Schönbrodt FD, Wagenmakers EJ. A tutorial on Bayes factor design analysis using an informed prior. *Behav Res Methods* 2019;51:1042–58.
96. Almeida DM, Rush J, Mogle J, Piazza JR, Cerino E, Charles ST. Longitudinal change in daily stress across 20 years of adulthood: Results from the national study of daily experiences. *Dev Psychol* 2023;59:515–23.
97. Cohen S, Janicki-Deverts D. Who's stressed? Distributions of psychological stress in the United States in probability samples from 1983, 2006, and 2009: psychological stress in the U.S. *J Appl Soc Psychol* 2012;42:1320–34.
98. Damoiseaux JS, Beckmann CF, Arigita EJS, Barkhof F, Scheltens Ph, Stam CJ, et al. Reduced resting-state brain activity in the “default network” in normal aging. *Cereb Cortex* 2008;18:1856–64.
99. Jockwitz C, Caspers S. Resting-state networks in the course of aging—differential insights from studies across the lifespan vs. amongst the old. *Pflugers Arch* 2021;473:793–803.
100. Varangis E, Habeck CG, Razlighi QR, Stern Y. The effect of aging on resting state connectivity of predefined networks in the brain. *Front Aging Neurosci* 2019;11:234.
101. Birn RM, Molloy EK, Patriat R, Parker T, Meier TB, Kirk GR, et al. The effect of scan length on the reliability of resting-state fMRI connectivity estimates. *Neuroimage* 2013;83:550–8.
102. Patriat R, Molloy EK, Meier TB, Kirk GR, Nair VA, Meyerand ME, et al. The effect of resting condition on resting-state fMRI reliability and consistency: a comparison between resting with eyes open, closed, and fixated. *Neuroimage* 2013;78:463–73.
103. Zou Q, Miao X, Liu D, Wang DJJ, Zhuo Y, Gao JH. Reliability comparison of spontaneous brain activities between BOLD and CBF contrasts in eyes-open and eyes-closed resting states. *Neuroimage* 2015;121:91–105.
104. James G, Witten D, Hastie T, Tibshirani R. *An Introduction to Statistical Learning: With Applications in R*. New York: Springer; 2014:426.
105. Cawley GC, Talbot NLC. On over-fitting in model selection and subsequent selection bias in performance evaluation. *J Mach Learn Res* 2010;11:2079–107.
106. Tervo-Clemmens B, Marek S, Chauvin RJ, Van AN, Kay BP, Laumann TO, et al. Reply to: multivariate BWAS can be replicable with moderate sample sizes. *Nature* 2023;615:E8–12.